Oil & Gas Science and Technology – Rev. IFP, Vol. 61 (2006), No. 1, pp. 25-42

Dossier

Development and Control of Combustion Systems
Évolutions et contrôle des systèmes de combustion

Mixture Preparation and Combustion in an Optically-Accessible HCCI, Diesel Engine

J. Kashdan[1] and G. Bruneaux[1]

1 Institut français du pétrole
1 et 4, avenue de Bois-Préau, 92852 Rueil-Malmaison Cedex - France
e-mail: julian.kashdan@ifp.fr, gilles.bruneaux@ifp.fr

Résumé — La préparation du mélange et de la combustion dans un moteur Diesel, HCCI à accès optique — Des techniques de fluorescence induite par laser (LIF) ont été appliquées afin d'étudier les procédés de préparation du mélange et de combustion dans un moteur monocylindre HCCI à accès optique. En particulier, l'influence de la géométrie de la chambre de combustion sur la répartition du mélange et sur la combustion a été étudiée. Un nouveau concept de piston à accès optique a permis l'application des diagnostics LIF à l'intérieur de la chambre de combustion. La LIF exciplex a été utilisée afin de caractériser la distribution de la phase liquide et de la phase vapeur du carburant. Par la suite, une étude détaillée des deux étapes de la combustion HCCI, flamme froide et combustion principale a été réalisée grâce à une combinaison de visualisation directe de la chimiluminescence, de LIF de l'espèce intermédiaire formaldéhyde (CH_2O) qui est présent pendant la flamme froide et puis de LIF du radical OH, qui est présent dans les zones de réaction et de gaz brûlés à température élevée. Enfin, des mesures par spectromètre ont été effectuées dans le but de déterminer l'origine des espèces du signal de chimiluminescence. Les expériences ont été réalisées dans un moteur monocylindre optique, équipé d'un système d'injection directe common rail et d'injecteur à angle de nappe réduit.

Les résultats présentés mettent en évidence le rôle important de la géométrie de la chambre de combustion sur la préparation du mélange et les caractéristiques de combustion pour des stratégies d'injection tardives, surtout dans les cas où l'impact des jets est inévitable. Les résultats de LIF à 355 nm ont montré la présence de l'espèce intermédiaire de formaldéhyde, ce qui a permis de localiser temporellement et spatialement les précurseurs de l'auto inflammation dans la phase précédant l'apparition du signal de chimiluminescence. Les résultats ont mis en évidence que le CH_2O est rapidement consommé dès le début de la combustion principale, ce qui correspond au démarrage du dégagement d'énergie et à la première détection du radical OH. .

Abstract — Mixture Preparation and Combustion in an optically-accessible HCCI, Diesel Engine — *Planar laser-induced fluorescence (LIF) imaging techniques have been applied in order to study the mixture preparation and combustion process in a single cylinder, optically-accessible homogeneous charge, compression ignition (HCCI) engine. In particular, the influence of piston bowl geometry on the in-cylinder mixture distribution and subsequent combustion process has been investigated. A new optically-accessible piston design enabled the application of LIF diagnostics directly within the combustion chamber bowl. Firstly, laser-induced exciplex fluorescence (LIEF) was exploited in order to characterise the in-cylinder fuel spray and vapour distribution. Subsequently a detailed study of the two-stage HCCI combustion process was conducted by a combination of direct chemiluminescence imaging, laser-induced fluorescence (LIF) of the intermediate species formaldehyde (CH_2O) which is present*

during the cool flame and LIF of the OH radical which is subsequently present in the reaction and burned gas zones at higher temperature. Finally, spectrometry measurements were performed with the objective of determining the origin of the emitting species of the chemiluminescence signal. The experiments were performed on a single cylinder optical engine equipped with a direct-injection, common rail injection system and narrow angle injector.

The experimental results presented reveal the significant role of the combustion chamber geometry on the mixture preparation and combustion characteristics for late HCCI injection strategies particularly in such cases where liquid impingement is unavoidable. Planar LIF 355 imaging revealed the presence of the intermediate species formaldehyde allowing the temporal and spatial detection of auto-ignition precursors prior to the signal observed by chemiluminescence in the early stages of the cool flame. Formaldehyde was then rapidly consumed at the start of main combustion which was marked not only by the increase in the main heat release but also by the first detection of OH, present within the reaction and burned gas zones. In the case of the flat piston geometry, soot precursors were also detected, as indicated by the strong polycyclic aromatic hydrocarbon (PAH) fluorescence signal observed later in the cycle (from 375 CAD).

DEFINITIONS

CAD	Crank Angle Degree
CI	Compression Ignition
DI	Direct Injection
EGR	Exhaust Gas Recycle
FWHM	Full Width Half Maximum
HCCI	Homogeneous Charge Compression Ignition
IMEP	Indicated Mean Effective Pressure
LIEF	Laser Induced Exciplex Fluorescence
LIF	Laser Induced Fluorescence
LII	Laser Induced Incandescence
NADI	Narrow Angle Direct-Injection
PAH	Poly-aromatic Hydrocarbons
RoHR	Rate of Heat Release
ROI	Region of Interest
RPM	Revolutions per Minute
SI	Spark Ignition
SOI	Start of Injection
TDC	Top Dead Centre
TMPD	Tetramethyl-phenyldiamine.

INTRODUCTION

An improvement in thermal efficiency combined with significant reductions in NOx and soot emissions have been largely responsible for intensifying global research interest into Homogeneous Charge Compression Ignition (HCCI) combustion [1-3]. The HCCI engine is often regarded as a hybrid concept since it exploits both the principles of conventional spark-ignition (SI) and compression-ignition (CI) engines. HCCI combustion generally requires a pre-mixed, highly diluted and homogeneous charge. This charge is subsequently auto-ignited during the compression stroke and results in exothermic reactions which have been shown to initiate at multiple sites within the combustion chamber and at a relatively uniform, globally lean equivalence ratio. The majority of recent experimental HCCI studies have tended to employ an engine with a moderate compression ratio (typically 14:1) in which a highly diluted, pre-mixed charge is produced by gasoline fuel injection into a heated intake port thereby ensuring sufficient time to achieve mixture homogeneity. One of the major benefits of port-injected, pre-mixed HCCI combustion is that it is not limited by the rates of fuel atomisation, evaporation and mixing at the fuel/air interface which is in contrast to conventional direct injection Diesel engines since auto-ignition occurs whilst fuel is still being injected. In the latter case, combustion is inherently heterogeneous with fuel-rich zones existing in the non-premixed regions whilst the fuel-air charge essentially produces a number of turbulent diffusion flames. As a result, the locally fuel-rich core consequently burns at significantly higher temperatures which leads to higher levels of pollutant emissions such as NOx and soot. In contrast HCCI combustion is dominated to a large extent by local chemical-kinetic reaction rates while it has also been proposed that turbulence effects probably have little direct effect although local temperature variations might have a secondary influence since the chemical reaction rates are very sensitive to temperature [4].

In order to limit the rate of combustion and minimise peak combustion temperatures which contribute significantly to reducing the engine-out NOx and soot emissions, highly diluted mixtures are generally required for HCCI combustion and this is achieved by using either internal (residual gas trapping) or external exhaust gas recirculation (EGR). In contrast to diffusion-limited combustion the absence of locally fuel-rich regions limits the formation of soot. However, if injection timing is not optimised and leads to liquid fuel impingement on relatively cool combustion chamber surfaces, fuel-rich regions can be formed prior to combustion which could potentially result in greater engine-out emissions

such as HC and soot. In the present study, HCCI combustion has been investigated on a direct-injection Diesel engine operating at a reduced compression ratio with a highly diluted intake charge in order to limit the combustion rate. Although the ultimate objective would be to employ HCCI combustion over the complete engine operating range the general consensus is that a combined approach must be adopted, employing HCCI strategies at low or part load whilst reverting to conventional direct-injection (diffusion-limited combustion) to satisfy full load requirements. The advantages of this latter approach is that existing common rail fuel injection systems can be employed as is the case in the present study however the fuel injection process (*i.e.* fuel injection rate, atomisation and evaporation) then becomes paramount to successful HCCI operation particularly for late injection strategies during the compression stroke. The experiments described made use of a conventional injector with an optimised multi-hole nozzle (NADI^{TM} concept) producing narrow angle jets [9].

Most fuels employed in HCCI, especially those with a low-octane number display an extended pre-combustion phase or so-called "cool flame" prior to the development of the main combustion phase. During this phase, exothermic reactions cause the formation of high levels of partially oxidised hydrocarbon compounds such as aldehydes; the regions of auto-ignition and the early cool flame can be localised by these species [5]. The main or "high temperature" combustion phase which follows the cool flame is characterised by a rapid rate of heat release. Chemiluminescence imaging of the naturally-emitted light is generally employed as a useful means of locating, both temporally and spatially the auto-ignition site(s) and the subsequent combustion process. However, as explained in Ref. [6], chemiluminescence emission occurs at specific wavelength bands which corresponds to the photo-emitting molecules and the signal is often relatively weak, particularly during the early stages of auto-ignition and also suffers from a lack of spatial resolution since the image is integrated along the line-of-sight. In the present study, a new optically-accessible piston has permitted the application of two selective planar LIF techniques; LIF of the OH radical at an excitation wavelength near 283 nm and LIF at 355 nm. The first technique allows the visualisation of the OH radical which is present in the reaction and burned gas zones at elevated temperature whilst the LIF 355 technique has been applied in order to visualise the intermediate species formaldehyde which is produced as a result of fuel decomposition during the cool flame. These two LIF techniques ultimately allow us to obtain more detailed information on the auto-ignition and two-stage HCCI combustion process. The LIF visualisations allow a detailed study of the combustion process and in particular the excitation of intermediate species such as formaldehyde which is present during the low temperature cool flame and poly-aromatic hydrocarbons (PAH), the precursors of soot. LIF imaging of the OH radical, which is present in both the reaction and burned gas zones during the subsequent high temperature combustion phase has also been performed whilst both these techniques have been complemented by direct chemiluminescence imaging and spectrally resolved measurements of the naturally emitted light.

It is generally proposed that HCCI combustion could be implemented at part or low-load operating regimes whilst at full load, conventional direct injection (heterogeneous) strategies have to be adopted [8, 9]. HCCI combustion via direct injection strategies is generally achieved through early injection strategies to ensure the production of a homogeneous air-fuel mixture. However, one of the major problems associated with direct-injection HCCI combustion strategies is that the very low in-cylinder pressures encountered for early injection strategies leads to excessive fuel jet penetration and subsequent wall wetting which is detrimental to engine-out emissions. In an attempt to resolve this issue, the NADI^{TM} concept has been developed in which the objective is to achieve HCCI combustion via late (near to TDC) direct-injection strategies and the use of an optimised combustion chamber geometry to improve mixture homogeneity. This paper reports an investigation into the effects of piston geometry on the in-cylinder fuel/air mixture distribution and combustion development for late injection strategies which have been conducted in an optically accessible direct injection HCCI Diesel engine. Figure 1 shows a schematic view of the two piston geometries which are subsequently referred to in the text as the flat piston and bowl-dome piston geometries.

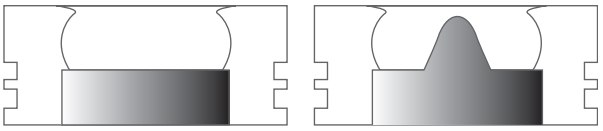

Figure 1

Schematic diagram of the flat piston (LHS) and bowl-dome piston (RHS) geometries.

1 EXPERIMENTAL SETUP

1.1 Optical Engine

The experiments were performed in an optically accessible, single cylinder, direct-injection Diesel engine operated in HCCI mode which was equipped with a 4 valve cylinder head and re-entrant bowl shaped piston. An extended piston was used in order to accommodate a 45° mirror enabling either combustion chamber illumination and/or light collection via a piston-crown quartz window as illustrated in Figure 2. To

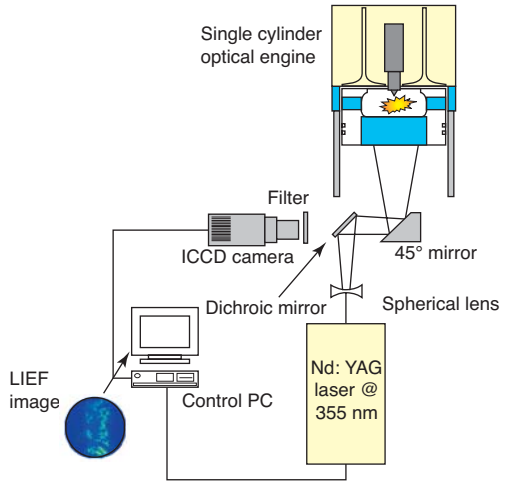

Figure 2

Schematic diagram of the experimental arrangement used for liquid and vapor phase visualizations in the piston bowl by laser-induced exciplex fluorescence (LIEF).

limit the rate of combustion, a large squish height was set in order to operate the engine at a low compression ratio (14:1) and avoid early auto-ignition of the fuel/air mixture. The optical engine was operated at 1200 rpm to ensure synchronisation with the 10 Hz repetition rate of the Nd:YAG laser. An optical angular encoder (BEI M25) with 0.1 CAD resolution allowed synchronisation of the camera and laser with respect to the engine cycle whilst in-cylinder pressure was measured at 0.1 CAD increments via a pressure transducer (Kistler 6053C60) and typically ensemble-averaged over 200 engine cycles. Table 1 summarises the engine specifications. Experiments were conducted once the engine cylinder had been pre-heated by means of a water jacket to a stable temperature of 50°C. In order to maintain relatively long periods of continuous operation and to minimise the rate of window fouling, the experiments were performed with the engine fired once every 5th engine cycle. The skip firing sequence also ensured the admission of a fresh fuel/air mixture to the engine by eliminating the effects of trapped exhaust gas residuals from the previous cycle thus providing well-defined in-cylinder conditions at BDC. EGR was simulated by the admission of pure nitrogen acting as the charge diluent. The flowrates of the intake air and nitrogen were measured via the use of two sonic flow nozzles.

A high-pressure common-rail injection system supplied dodecane fuel at a nominal rail pressure of 1100 bar. A 6 hole nozzle (hole diameter/length of 0.120 mm/1 mm) with a narrow angle spray angle (less than 70°) was used. The combustion visualisations, planar LIF 355, LIF OH and spectrometry experiments were all performed for a late HCCI injection strategy with SOI at 357 CAD and an injected fuel quantity of 16 mm^3. The engine operating conditions are outlined in Table 2 below and show that the EGR level and global equivalence ratio were maintained at the same levels for both combustion chamber geometries.

TABLE 1

Specifications of the optical engine

Engine base type	2 liter, DI Diesel
Cycle	4-stroke
Number of cylinders	1
Number of valves	2 intake + 2 exhaust
Bore/stroke	85/88 mm
Displacement volume	0.5 l
Bowl diameter/depth	46/5 mm
Squish height	1.94 mm
Compression ratio	14
Intake pressure	1 bar (absolute)
Swirl number	2.2

TABLE 2

Engine combustion operating conditions

	EGR (%)	IMEP (bar)	Equivalence ratio
Flat piston	45	2.0	0.73
Bowl-dome piston	45	2.6	0.73

1.2 Laser Induced Exciplex Fluorescence

Planar laser-induced exciplex fluorescence (LIEF) imaging allowed qualitative visualisation of the mixture distribution within the piston bowl. The LIEF technique allows the simultaneous visualisation of both the liquid and vapour phases through the use of exciplex forming dopants as described by Melton [10, 11]. The selected dopants should ideally have similar vaporisation properties to the base fuel whilst producing a satisfactory fluorescence yield. In the present study, the base fuel, n-decane (boiling point of 174°C) was doped with 1-methyl-napthalene and a small quantity of TMPD whilst appropriate spectral filters permitted separation of the two fluorescence signals. In order to minimise the effects of oxygen-induced quenching which can significantly reduce the fluorescence signal for the vapour phase the experiments were performed in a 100% nitrogen environment. The boiling points of TMPD (260°C) and naphthalene (218°C) correspond to the middle points of diesel fuels and thus they are well suited to the study of diesel sprays. Optical access into the cylinder was provided by a transparent quartz piston window and a 45° mirror as shown in Figure 2. The laser beam from a frequency-tripled

Nd:YAG laser ($\lambda = 355$ nm) was passed through a divergent spherical lens ($f = 35$ mm) allowing global illumination of the combustion chamber. The fluorescence signal was then captured by a 16 bit image-intensified CCD camera (Princeton instruments PIMAX, 1024 x 1024 pixel array) equipped with a UV lens (Nikkor 105 mm).

1.3 Planar Lif of Combustion Radicals

The experimental set-up employed for the measurement of OH in the optical engine is shown in Figure 3. A 650 mJ pulse from a Nd:YAG laser (Continuum Lasers Precision II) at a wavelength of 532 nm and 10 Hz repetition frequency was used to pump a tuneable dye laser (Continuum Lasers ND 6000) which contained a solution of Rhodamine 590 dye. A BBO crystal allowed frequency doubling of the output beam of the dye laser permitting excitation of the OH radical in a wavelength range which was tuneable between 280 and 284 nm. The experiments reported in the present study were conducted at an excitation wavelength of 282.93 nm corresponding to the Q1(6) transition of the $A^2\Sigma^+$-$X^2\Pi^+$ system. The available laser energy after frequency doubling was typically 30 mJ although further losses due to the combination of optical components resulted in a measured laser energy within the combustion chamber of about 15 mJ. The incident light sheet formed within the piston bowl had a width and thickness of approximately 20 and 0.5 mm respectively. The fluorescence signal was captured by a 16 Bit image-intensified CCD camera (Princeton instruments PIMAX, 512 x 512 pixel array) equipped with a UV lens (Cerco, 45 mm, f/1.8). In order to maximise the amount of light collected, full camera gain and lens aperture were required throughout the experiments. The image intensifier duration was maintained constant with an opening duration of 10 ns.

In order to isolate the OH fluorescence signal (at approximately 310 nm) from interference caused predominantly by laser elastic scattering, PAH fluorescence and soot particle incandescence [12], a combination of optical filters were placed into the optical path of the camera which consisted of a band pass filter (FWHM of 16 nm) centred on 312 nm and a 358 nm low pass filter. As shown in Figure 3 the laser sheet was passed through the sapphire crown and entered the piston bowl via one of the quartz window inserts. It was necessary to add a second, diametrically opposed window insert to allow the laser sheet to exit the bowl, thereby avoiding reflections of the incident light sheet which would otherwise interfere with the fluorescence signal. In order to confirm whether the fluorescence signals detected were indeed solely due to the presence of OH and not other fluorescing species, images were also acquired at a non-resonant or "off-line" wavelength of 282.80 nm. Figure 4 shows a comparison between two single-shot LIF OH images obtained at "on-line" (resonant) and "off-line" (non-resonant)

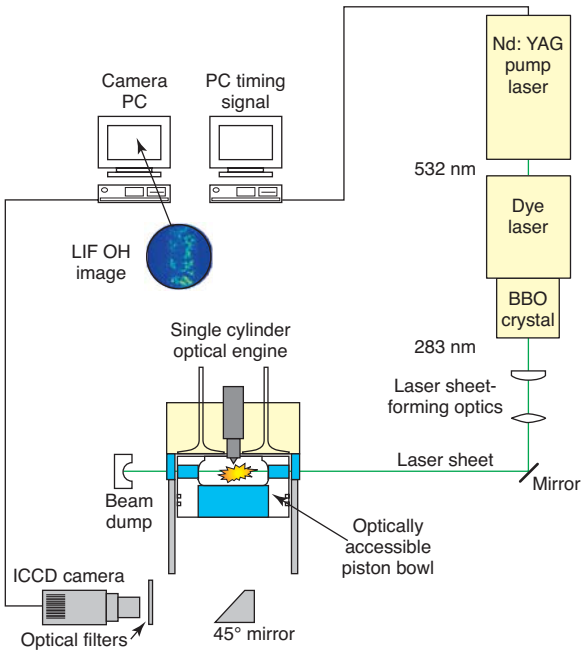

Figure 3

Schematic diagram of experimental arrangement for planar LIF OH measurements in the piston bowl of a single cylinder HCCI Diesel engine.

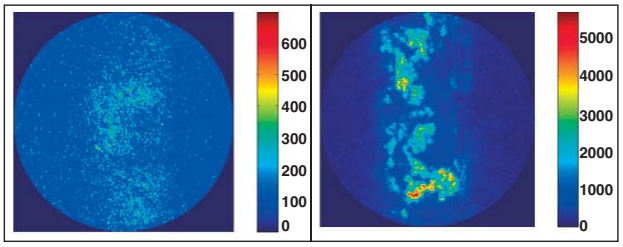

Figure 4

Typical single-shot planar LIF OH images obtained at non-resonant wavelength (LHS) and resonant wavelength (RHS).

wavelengths which not only confirms that the fluorescence signal was indeed due to the detection of the OH radical but also that the filters used were effective in minimising signal interference due to elastic laser scattering and other species which might fluoresce at the same wavelength.

Planar LIF measurements were also performed by employing a frequency-tripled Nd:YAG laser which provides excitation at a wavelength of 355 nm. The principal objective was to excite the fluorescence of formaldehyde which is intermediately present within the cool flame. Excitation at a wavelength of 355 nm does present a number of drawbacks however. Firstly, this particular wavelength only allows excitation of weak transitions in the CH_2O molecule [7] and unlike selective wavelength excitation [13], does not allow

the discrimination of the formaldehyde signal against non-resonant signal contributions, notably from the fluorescence of PAH [14]. The experimental set-up was largely similar to that described above for the LIF OH measurements, the only difference being the excitation wavelength and thus the replacement of the dye laser by the Nd:YAG laser. A different set of optical filters was used in order to isolate the LIF 355 signal which consisted of a 465 nm bandpass filter (FWHM 70 nm) and a 435 nm high-pass filter. The laser energy was maintained at approximately 80 mJ which provided a very satisfactory signal to noise ratio whilst being sufficiently low enough to prevent laser-induced incandescence (LII) of soot particles which would likely interfere with the desired fluorescence signal. For both the LIF 355 and LIF OH techniques, ensemble-averaged images were calculated from 100 single-shot images which were acquired from successive engine firing cycles at a given engine crank angle.

1.4 Combustion Imaging and Spectrometry

The temporal and spatial development of the HCCI combustion process within the piston bowl was visualised by direct imaging of the naturally emitted light using a 16-bit intensified CCD camera and 45 mm UV lens (Cerco). The spectral characteristics of the naturally emitted light and its temporal evolution during the combustion process were subsequently measured by a spectrometer (Acton Research SpectraPro, 300 lines/mm grating). The emitted light was collected by a collimating lens (f = 500 mm) and then focused (f = 100 mm) onto the slit of the spectrometer (250 mm entrance slit) which was coupled to the ICCD camera. A mercury-vapour lamp was used to calibrate the spectrometer to known wavelengths. In order to maximise the collected light intensity at a specific crank angle, emission spectra were typically accumulated over 100 consecutive engine cycles.

1.5 Image Interpretation and Post-Processing

In-house image post-processing routines were developed and applied to the acquired images for example in order to determine the ensemble-averaged and standard deviation images at different engine crank angle positions. The image processing routine enables the rejection of "erroneous" images which might be either underexposed or overexposed (saturated). Furthermore, in order to account for the wide variations in natural light emission which is generally weak during the early chemiluminescence period and can be orders of magnitude greater later during the cycle due to soot incandescence, the intensifier gate duration (exposure time) had to be varied. However, the post-processing routine used in the present study accounted for variations in either the camera gain setting or intensifier gate duration since the camera sensitivity was previously calibrated thus permitting at least a semi-quantitative analysis of the images acquired.

The planar light sheet visualisations performed (*i.e.* LIF OH and LIF 355) posed particular problems near to TDC for the bowl-dome geometry as a result of very intense reflections produced by the incident laser sheet on the dome. As shown in Figure 5, the resulting images were inevitably saturated by these reflections and thus dominated any fluorescence signal that may have been present. In order to resolve this issue, two regions of interest (ROI) were selected within the image, either side of the dome. Figure 5 shows a typical LIF OH image which reveals the laser sheet reflections, the two ROI's selected and the resulting LIF image.

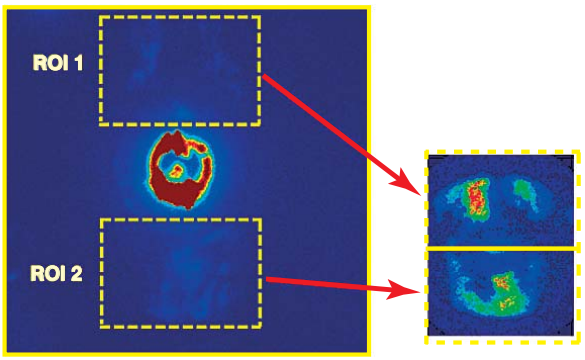

Figure 5

Saturated LIF OH image (LHS) due to reflections from the bowl-dome and the resulting image (RHS) obtained via selection of the 2 defined regions-of-interest (ROI).

2 RESULTS AND DISCUSSION

2.1 Fuel Mixture Distribution

Visualisations of the in-cylinder fuel and vapour distributions obtained via laser induced exciplex fluorescence are shown in Figure 6 for the flat piston geometry. In this particular case, the start of fuel injection as defined by the command signal was 320 CAD although taking into account the hydraulic and electromechanical injector delay time, liquid fuel typically appears 2 CAD later. Although this SOI timing is not particularly considered to be typical of a "late" HCCI injection strategy the results presented are useful as a means of explaining the general characteristics of the in-cylinder temporal spray and vapour development and more importantly provide a context to the subsequent combustion data presented and discussed later in the paper. One observes from both the liquid and vapour phase images that global spray symmetry of the six fuel jets is well maintained and

there does not appear to be a significant effect of in-cylinder swirl. At 327 CAD, Figure 6 clearly shows that liquid fuel impinges on the piston face whilst the corresponding vapour phase images acquired at 327 and 330 CAD tend to indicate a certain degree of fuel stratification through the formation of a fuel rich region which appears to be confined to the centre of the piston following fuel impingement. Such trends would be further exacerbated for even later SOI timings closer to TDC and maintaining the narrow spray angle, fuel impingement would inevitably occur closer to the centre of the piston bowl.

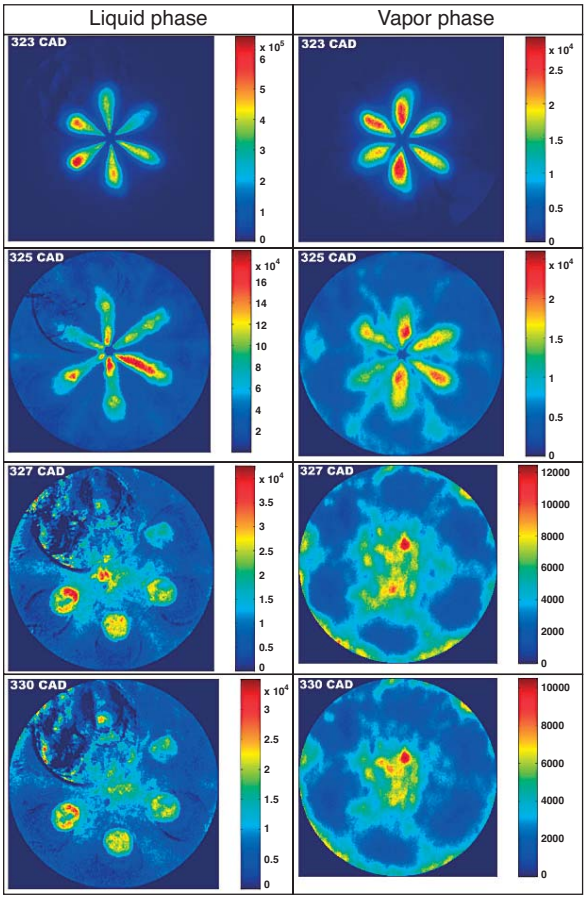

Figure 6

Temporal evolution of the fuel distribution within the piston bowl (liquid and vapor phase) for the flat piston geometry (SOI = 320 CAD).

Although LIEF images of the fuel distribution for the bowl-dome geometry are not presented here, recent 3D CFD data reported in Ref. [16] have shown that the bowl-dome piston geometry has a significant effect on the fuel distribution for late injection timings. As illustrated in Figure 7, during the early stages of injection, the narrow angle fuel jets propagate downwards in the vicinity of the bowl-dome, each of the jets effectively shrouding the dome. Although liquid impingement is unavoidable, the bowl-dome geometry guides the fuel vapour jets in a radial direction towards the re-entrant bowl wall. For late injection strategies near to TDC, the fuel mixture is recirculated by the re-entrant and it appears as though the fuel mixture is confined by the cylinder head. The mixture subsequently disperses radially into the squish zone and also back towards the centre of the piston. Figure 7 seems to indicate that recirculation of the fuel mixture by the bowl-dome and reentrant results in more efficient utilisation of the available air which is believed to significantly improve mixture homogeneity. More importantly, the production of a locally fuel-rich zone due to liquid impingement on the piston surface as was observed in the case of the flat piston *(Fig. 6)* is avoided. The bowl-dome piston effectively "guides" the fuel mixture towards the re-entrant thereby enhancing air-fuel mixing which subsequently helps to improve mixture homogeneity.

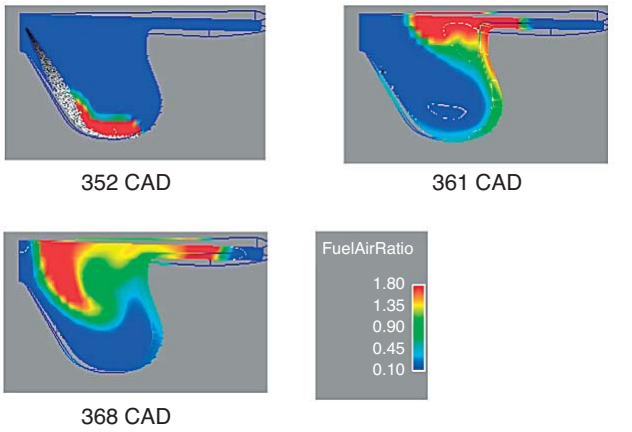

Figure 7

Calculated temporal evolution of the fuel distribution within the piston bowl (liquid and vapor phase) for the bowl-dome piston geometry (from Ref. [16]).

2.2 Combustion Imaging

As described earlier, HCCI combustion consists of two distinct stages, the first stage corresponds to the early cool flame in which chain-branching oxidation reactions take place at relatively low temperature. It has been shown that these pre-combustion reactions are highly sensitive to pressure and temperature conditions in addition to in-cylinder gas composition and fuel formulation [4, 24-26]. Following auto-ignition, the second stage begins and corresponds to the main combustion in which much higher in-cylinder temperatures are attained. In order to study in greater detail the physical-chemical processes which occur during HCCI

Diesel combustion, laser-based combustion diagnostics have been exploited in order to excite the fluorescence of selected radicals which are formed during combustion. The planar LIF 355 technique allows the visualisation of reaction precursors and partially oxidised hydrocarbon compounds such as formaldehyde which exist at relatively low temperature during the cool flame phase. In addition, visualisation of the OH fluorescence signal allows the location of both the reaction and burned gas zones and has previously been applied for the study of Diesel jet diffusion flames [12]. Prior to the application of the PLIF techniques, the combustion process was first of all characterised by in-cylinder pressure analysis and chemiluminescence imaging for the two piston geometries as a means of understanding the combustion temporal development, homogeneity and in particular the potential location of soot-forming zones. Figure 8 shows a comparison of the in-cylinder pressures (LSH) and heat release rates (RHS), the latter having been calculated via the 0-D thermodynamic analysis as described in Ref. [17]. One observes several notable differences according to the piston geometry.

Firstly, the combustion phasing is clearly different. Following the end of injection, the delay associated with the early cool flame period (which does not result in a significant increase in the measured in-cylinder pressure) and prior to the main pressure rise is noticeably greater for the bowl-dome piston geometry occurring at approximately 375 CAD compared with 371 CAD for the flat piston geometry. As a result of the retarded combustion phasing the peak in-cylinder pressure attained in the former case is inevitably lower at 32 bar compared to 36 bar for the flat piston due to the fact that combustion occurs later into the expansion stroke. The in-cylinder pressure traces indicate that the combustion phasing is retarded as a result of an increased auto-ignition delay in the case of the bowl-dome geometry. The corresponding heat release rates also clearly reveal the effect of piston geometry, the small initial peak corresponding to the cool flame stage which starts to rise at about 365 CAD for the flat piston is delayed several CAD in the case of the bowl-dome geometry. Subsequently, the main heat release for the flat piston occurs well in advance to that of the bowl-dome piston and furthermore a comparison of the gradients of the main heat release curves suggests that the rate of heat release is slightly lower in the latter case. These results illustrate the significant influence of the piston bowl geometry on the auto-ignition delay and consequently the pressure-rise rate and peak in-cylinder pressures attained. It is possible that the longer auto-ignition delay in the case of the bowl-dome geometry is due to differences in the fuel-air mixing process.

Figures 9 and 10 show temporal sequences of the ensemble-averaged combustion images corresponding to the flat piston geometry and bowl-dome piston geometry respectively. Although ignition is usually considered to occur at the first detectable combustion-induced pressure rise, it is well known that a certain degree of natural flame emission occurs prior to this which is relatively weak and is due to chemiluminescence [6]. Indeed the measured in-cylinder pressure signals did not reveal a significant rise until approximately 371 and 375 CAD for the flat and bowl-dome geometries respectively. Meanwhile the chemiluminescence signal, although initially very weak in intensity appears to confirm the presence of auto-ignition precursors from approximately 363 CAD onwards. The subsequent images obtained at 365 CAD reveal the early stages of combustion which, according to the heat release rates *(Fig. 8)* occur at relatively low temperature. In the case of the flat piston *(Fig. 9)* one observes rapid combustion propagation which appears to occur within the pre-mixed vapour clouds of the six fuel jets almost reaching the piston bowl wall. In contrast

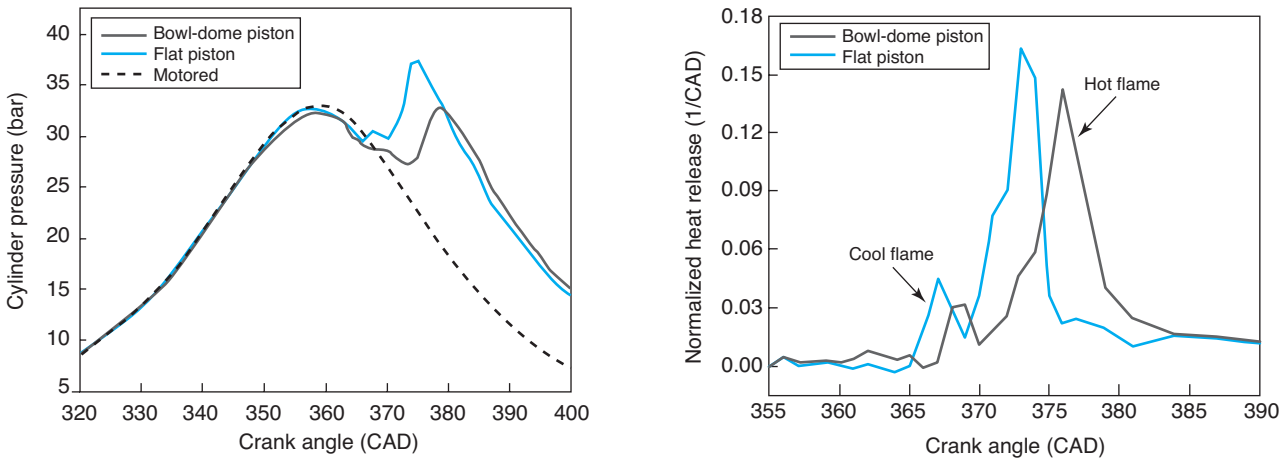

Figure 8

Comparison of in-cylinder pressure (LHS) and normalized heat release rates (lRHS) for the two piston geometries tested.

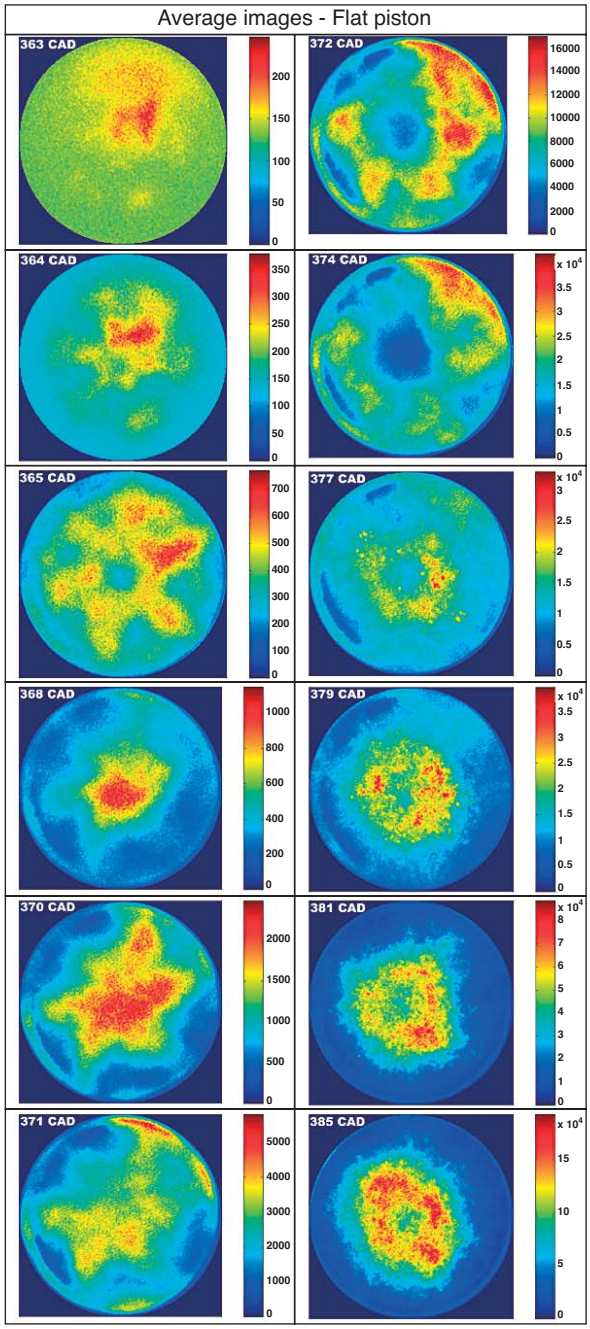

Figure 9

Ensemble-averaged combustion images for the flat piston geometry (CAD given in frame title).

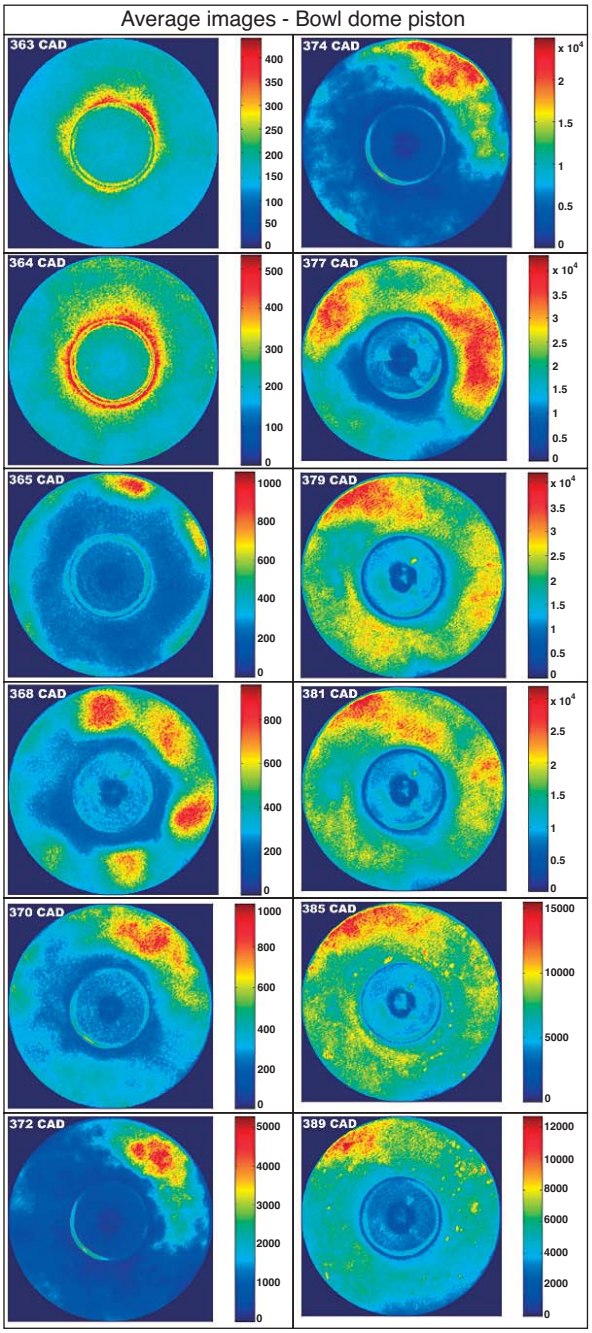

Figure 10

Ensemble-averaged combustion images for the bowl-dome piston geometry (CAD given in frame title).

however, for the bowl-dome combustion chamber geometry at 365 CAD the strongest chemiluminescence signal is located in several discrete regions around the periphery of the bowl near to the re-entrant suggesting that the pre-mixed fuel vapour cloud has penetrated further into the piston bowl by virtue of fuel having been "guided" by the dome. This correlates well with the LIEF image sequences discussed earlier. At 368 CAD, further differences are again observed in terms of the spatial location of the chemiluminescence signal for the two pistons. In the case of the flat piston, measured luminous intensity is clearly highest in the centre of the bowl and combustion at this stage appears to remain largely confined to this region before spreading out radially towards the bowl walls at 371 CAD. In contrast, the effect of

the dome clearly distributes the mixture towards the bowl wall and the corresponding image acquired at 368 CAD confirms this, the signal being most intense around the periphery of the bowl and apparently associated with the fuel-rich vapour clouds formed by the six fuel jets. This early cool flame period is characterised by weak chemiluminescence intensities which is confirmed for both piston geometries and lasts until approximately 373/374 CAD. Further discussion is given later in this section of the paper when analysing quantitatively the evolution of the luminous signal.

The start of the main combustion phase can be identified by the transition which is observed firstly, from the rise in the in-cylinder pressure signal after approximately 373 CAD and secondly, by observing the combustion images, particularly in terms of the image intensity *(Figs 9 and 10)* and in the present case shows a rapid increase by as much as two orders of magnitude after 373 CAD. The high temperature combustion stage is characterised by a significant increase in luminous intensity and considering firstly the flat piston geometry, Figure 9 reveals an intense zone clearly observed in the near wall region around the periphery of the piston bowl until about 377 CAD with an apparent void in the centre. From 377 CAD onwards, a third phase of the combustion development can be identified, associated with low heat release in which a locally rich zone appears and remains largely confined to the centre of the piston. This rich zone is characterised by high intensities typical of the black body type radiance produced during sooting combustion which subsequently increases during the latter stages of the combustion process. The intense signal due to the presence of soot most likely originates from a locally fuel-rich zone formed as a result of fuel impingement during injection some 15 CAD earlier. Following fuel impingement on the piston surface the locally fuel-rich mixture subsequently evaporates and has the effect of stratifying the in-cylinder charge. The effects of local fuel stratification are believed to be largely responsible for the advanced ignition timing observed for the flat piston geometry which was confirmed earlier by in-cylinder pressure data and heat release rates since the local mixture composition is known to have a significant influence on the cool flame oxidation reactions as discussed earlier. Furthermore, the peak in-cylinder combustion pressures and temperatures are clearly higher in the case of the flat piston geometry and thus one would expect to observe increased levels of engine-out emissions of soot and NOx (the formation of both these pollutant species being directly coupled to peak temperature). These observations are discussed in further detail with respect to the LIF 355, LIF OH and spectrometry measurements which are described in subsequent sections in this paper.

In the case of the bowl-dome piston geometry *(Fig. 10)*, autoignition occurs at approximately 373/374 CAD. The subsequent main combustion phase is characterised by a significant increase in luminous intensity which correlates well with the main heat release *(Fig. 8)*. From 379 CAD onwards, the images obtained tend to indicate that combustion is globally more homogeneously distributed and is primarily believed to be due to the improved mixture preparation as discussed earlier. Furthermore, the effect of the dome would perhaps enhance or at the very least help to maintain the level of air swirl generated within the piston bowl which may further help to improve mixture homogeneity. The trends observed in the above image sequences can also be expressed in terms of the average image intensity as shown in Figure 11 which is useful in identifying the evolution of combustion and which has been shown to be approximately proportional to the heat release [18]. The heat release rate is also plotted on the same figure for comparison. In comparing the heat release rate and mean combustion luminosity, Figure 11 confirms quantitatively just how weak the chemiluminescence signal is during the early stages of combustion prior to auto-ignition, yielding very low signal intensities during the cool flame which can be identified by the first, smaller peak of the heat release.

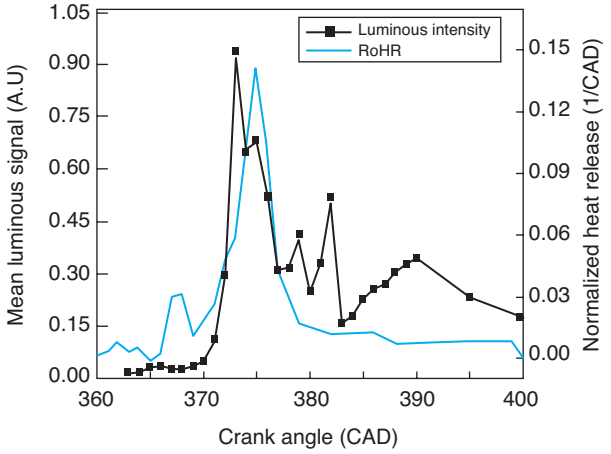

Figure 11

Comparison of mean chemiluminescence signal and normalized heat release.

2.3 LIF 355 Imaging

Figure 12 shows a temporal sequence of averaged and single-shot LIF 355 images for the flat piston geometry. Ensemble-averaged and single-shot images have been presented here since the former allows us to easily determine the spatial location of the LIF 355 signal over a number of engine cycles whilst the latter reveals in finer detail the structure of the fluorescing species which are "smoothed out" and thus not so well defined in the averaged image. For each image acquired the camera gain was maintained at the same level. With

reference to the images, the laser sheet entered the field of view from below and exited at the top. The single shot images shown in Figure 12 reveal that the first LIF 355 signal was detected at 361 CAD, consisting of small discrete pockets located in the centre of the bowl. The averaged image confirms that over successive cycles the LIF 355 signal is preferentially located in the centre of the piston bowl. If a comparison is made between the initial LIF 355 images obtained and those acquired by direct combustion visualisation *(Fig. 9)* it is clear that the LIF 355 signal is detected approximately 2 CAD (corresponding to 280 μs at 1200 rpm) in advance of the initial, weak chemiluminescence signal which is also detected in the centre of the piston bowl.

The LIF 355 signal not only reveals a much greater signal-to-noise ratio than that obtained by direct chemiluminescence but also the fluorescing species, which is almost certainly due to the presence of partially oxidised hydrocarbons such as formaldehyde appears to indicate the spatial location of the pre-cursors to auto-ignition. Similar findings have recently been reported in Diesel jet combustion studies performed in a high-pressure/temperature constant volume chamber [14]. The LIF 355 signal further increases at 364 and 368 CAD being detected throughout the illuminated plane within the piston bowl although remaining largely inhomogeneously distributed. At 371 CAD the signal intensity has clearly decreased but shortly afterwards increases for a second time from 376 CAD onwards, the LIF intensities increasing by an order of magnitude at 390 CAD. During these latter stages of the cycle, the fluorescence signal detected predominantly in the central region of the bowl most likely originates from the fluorescence of poly-aromatic hydrocarbons (PAH) which are the precursors of soot and can be explained by the following reasons; First of all, the intense LIF 355 signal observed late in the cycle correlates spatially with the signal detected by direct combustion visualisation *(Fig. 9)* which reveals several crank angle degrees later the presence of a locally rich zone which was characterised by very high luminous intensities located in the centre of the piston and is typical of soot incandescence. Secondly, the likelihood that the observed LIF 355 signal is due to the fluorescence of partially oxidised hydrocarbons such as aldehydes this late in the cycle is very small since they tend to be completely burned at higher temperature during the main combustion [7] and thirdly laser excitation at 355 nm has been shown to yield a strong PAH fluorescence signal [13, 14].

Figure 13 shows a temporal sequence of ensemble-averaged and single-shot LIF 355 images obtained for the bowl-dome piston geometry. As in the preceding case, it is useful to compare the LIF 355 images in relation to the temporal evolution of the images obtained by direct chemiluminescence *(Fig. 10)*. The first LIF 355 signal is detected just after TDC at 361 CAD and until 364 CAD is located around the periphery of the dome. However, interpretation of the LIF 355 signal obtained at this crank angle is not straightforward as it is likely that some signal contributions are due to laser sheet reflections from the dome. Further inspection of the images obtained later in the cycle between 366 and 374 CAD reveals a fluorescence signal in the same location although significantly weaker in intensity compared to the signal detected elsewhere within the piston bowl. Nevertheless, there appears to be a good correlation between the LIF 355 images obtained between 361 and 365 CAD and the chemiluminescence signal observed at similar crank angle positions in terms of the spatial location of the two signals, suggesting perhaps that the LIF 355 signal is indeed at least partly due to the fluorescence of reaction precursors such as formaldehyde.

At 365 CAD, the LIF 355 images reveal only a relatively small increase in the signal-to-noise ratio whilst discrete pockets corresponding to the fluorescence of the excited species are detected in the periphery of the bowl near to the re-entrant in agreement with the chemiluminescence images. One of the most notable differences observed in comparing the LIF 355 image sequences for the two piston geometries is that in the case of the bowl-dome piston geometry, the detected fluorescence signal is more homogeneously distributed (also shown clearly in the single-shot images) throughout the bowl during the cool flame stage. Later in the cycle, after the start of main combustion, from 375 CAD onwards the LIF 355 signal decreases to negligible levels as was observed in the case of the flat piston. This again strongly suggests that the fluorescence signal is due to the presence of reaction precursors such as formaldehyde which forms through low temperature oxidation during the early stages of the ignition process and during the cool flame prior to being completely consumed at the start of main combustion.

The major difference revealed by the LIF 355 images obtained for the bowl-dome piston geometry is the clear absence of any significant fluorescence signal during the latter stages of combustion (from 380 CAD onwards) which was previously observed in the case of the flat piston and attributed to the presence of PAH. The absence of significant PAH fluorescence is perhaps further evidence that the adoption of the bowl-dome geometry enhances mixture preparation and homogeneity which, as discussed earlier results in a longer auto-ignition delay. The increased ignition delay consequently limits the pressure rise rate and associated peak pressures and temperatures encountered which then appears to contribute to the reduction of soot precursors. Measurements of the engine-out smoke emissions using an *AVL* 415 smokemeter subsequently further confirmed these assertions and the results are tabulated below *(Table 3)*. It should be noted that for the engine-out emissions measurements the quartz optical components were replaced by equivalent metal components of identical geometry permitting engine operation without skip-firing. The results summarised in Table 3 below are in agreement with the experimental data obtained by chemiluminescence and LIF

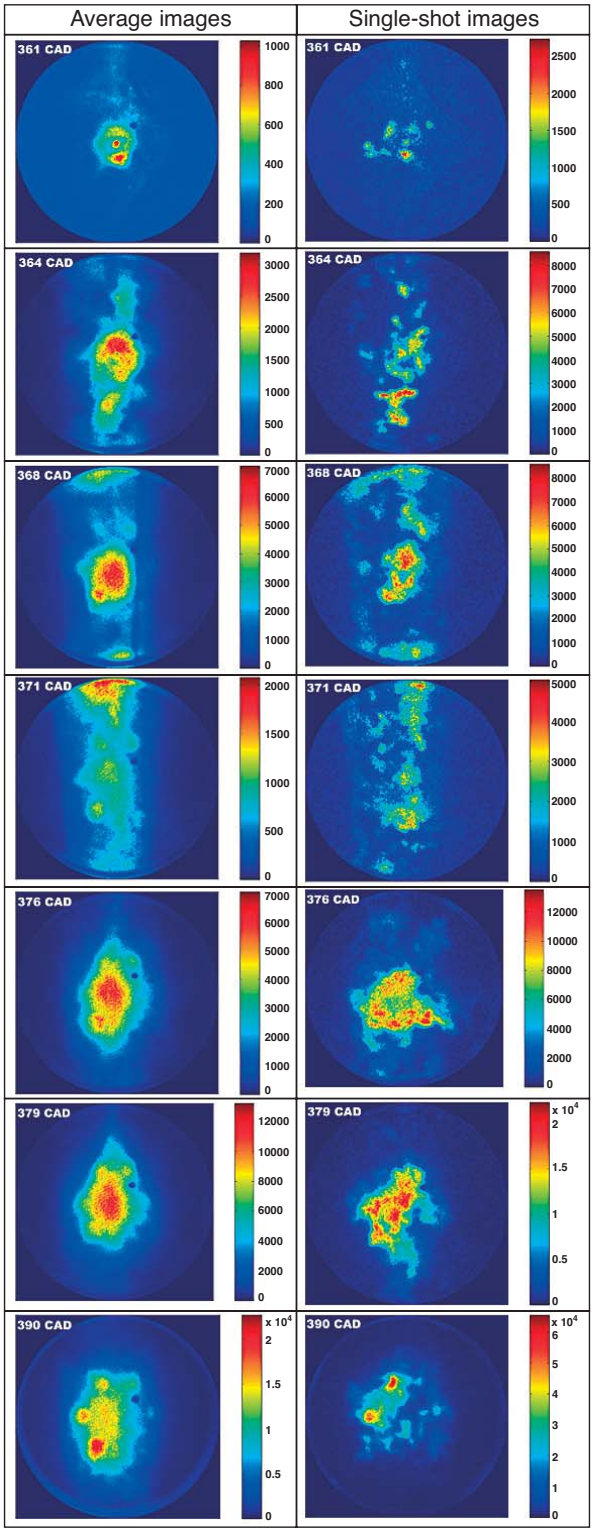

Figure 12

Ensemble-averaged and single-shot LIF 355 images for the flat piston geometry (CAD given in frame title).

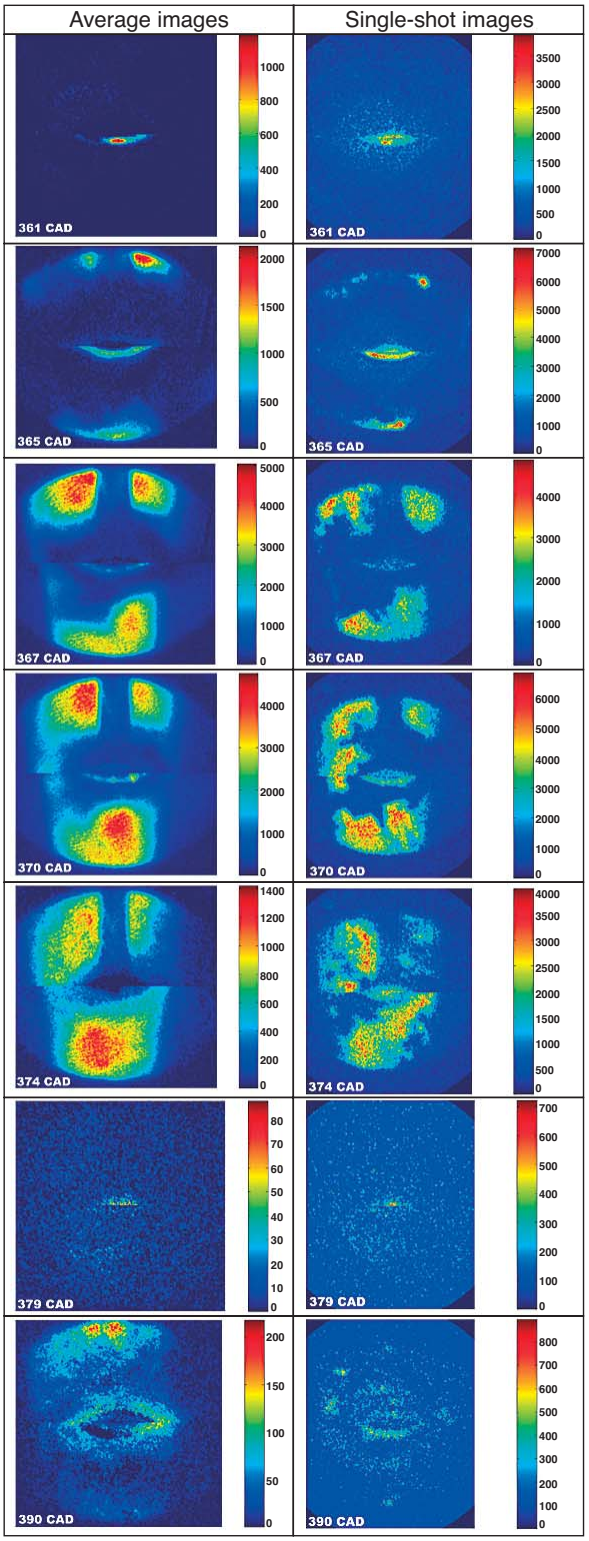

Figure 13

Ensemble-averaged and single-shot LIF 355 images for the bowl-dome piston geometry (CAD given in frame title).

355 imaging, revealing that for the flat piston geometry the measured smoke emissions were an order of magnitude greater in comparison with the bowl-dome geometry. Although the engine-out NOx emissions were similar, a significant increase in the CO emissions was observed for the flat piston geometry. The four-fold increase in CO emissions in the case of the flat piston geometry is almost certainly due to the production of locally fuel-rich zones within the combustion chamber as a result of the combined effects of liquid impingement and consequently non-optimum fuel-air mixing. The measured HC emissions in the case of the flat piston were also an order of magnitude greater than for the bowl-dome geometry which also appears to confirm that a large fraction of unburned fuel escapes combustion due to poor mixture preparation.

TABLE 3

Comparison of engine-out smoke, NO & CO emissions for the two different piston geometries

	Smoke (FSN)	NOx (ppm)	CO (ppm)
Flat piston	1.60	7.9	7610
Bowl-dome piston	0.13	8.5	1976

2.4 LIF OH Imaging

A temporal sequence of ensemble-averaged and single-shot planar LIF OH images obtained from within the optically-accessible piston bowl is presented in Figure 14 for the flat piston geometry. Images were obtained between 361 and 369 CAD but are not presented in the paper since, as expected, they simply confirm the absence of OH during the low temperature, cool flame stage. The very low signal-to-noise levels were similar to those revealed in the images obtained at 370 and 372 CAD. The first detection of LIF OH occurs at 373 CAD and the image signal-to-noise ratio clearly increases. The first detection of OH which is formed in the reaction and burned gas zones shows excellent temporal agreement with the heat release curves shown earlier in terms of marking the start of the main combustion phase. The single-shot images obtained reveal that the signal is inhomogeneous, characterised by small discrete pockets throughout the piston bowl. At 375 CAD, the LIF OH concentration increases within the illuminated plane although retains an inhomogeneous structure as depicted by the single-shot images. The averaged images shown from 375 CAD onwards clearly reveal that higher LIF OH signal intensities are detected on the laser sheet entry side of the bowl which initially suggests that the decrease in signal across the illuminated plane is due to laser sheet attenuation. However the apparent absence of LIF OH in the central region of the piston does not appear to be due to attenuation of the laser sheet since some signal, albeit weaker is detected in the upper part of the images at 378 CAD and onwards. The void observed in the centre appears to have increased significantly by 385 CAD and this perhaps suggests that any OH which was previously present in the central region of the piston has been removed by soot oxidation. Indeed, burner studies have shown that OH is important in soot oxidation and that the presence of soot and soot precursors tends to decrease OH concentrations [22]. This is in very good agreement with the findings presented and discussed earlier which confirmed, via LIF 355 imaging the presence of soot precursors (strong PAH fluorescence) and subsequently via direct imaging the characteristic black body type radiance typical of sooting combustion similarly located in the centre of the bowl.

Figure 15 shows a temporal sequence of averaged and single-shot LIF OH images corresponding to the bowl-dome piston geometry. Similarly to the results presented below for the flat piston, LIF OH initially appears in small discrete pockets at approximately 373 CAD. The signal-to-noise ratio subsequently increases however, the notable difference in comparing the LIF OH images of Figure 15 with those corresponding to the flat piston *(Fig. 14)* is that the spatial distribution of the OH fluorescence signal is clearly more homogeneous from 374 CAD onwards suggesting that both locally and globally, combustion develops more homogeneously throughout the chamber. The averaged images obtained between 374 and 381 CAD clearly reveal that part of the combustion chamber remained inaccessible by the laser sheet near to TDC due to the presence of the dome. However, much later in the cycle after TDC at 395 CAD, the piston dome no longer prevents laser sheet illumination in this region and a strong, homogeneous LIF OH signal can be observed. The presence of OH this late in the cycle suggests a much slower combustion rate and perhaps a longer phase of post-oxidation compared to the case of the flat piston in which the OH signal levels were observed to decrease rapidly to relatively low levels.

A more detailed analysis of the LIF 355 and LIF OH images is shown in Figures 16 and 17 which reveal the temporal evolution of the two LIF signals and illustrates more clearly the appearance of the signal peaks relative to one another and also in comparison to the heat release rates. Firstly, the upper graph in Fig. 16 for the flat piston geometry reveals that the initial small peak during the cool flame between 365 and 370 which has been shown to correlate with the presence of CH_2O shows very good agreement with the initial peak in the heat release curve prior to the start of the "hot" combustion. The main heat release starts at about 370 CAD and this corresponds to a marked decrease in the LIF 355 signal, indicating that the intermediate species is rapidly consumed due to the higher in-cylinder temperatures. The maximum heat release occurs at 375 CAD. As observed in the images, the LIF 355 signal increases for a second time peaking between approximately 383 and 390 CAD. The signal remains at elevated levels late into the cycle and as

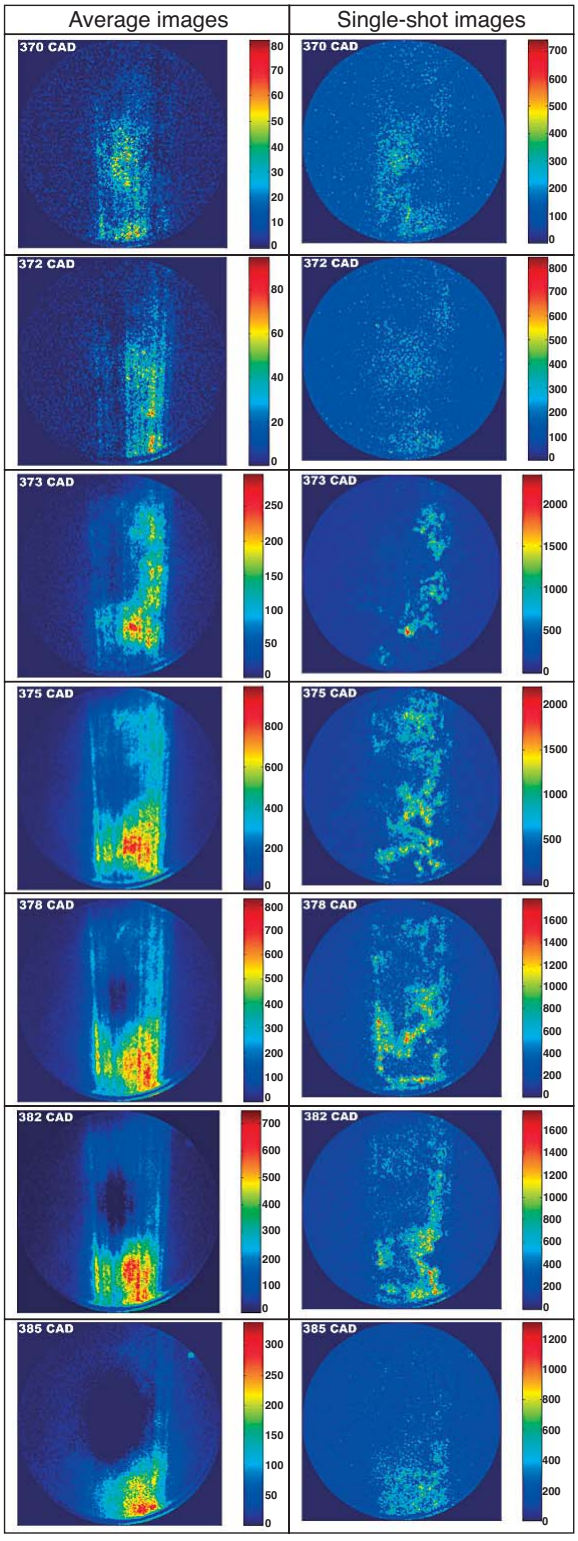

Figure 14

Ensemble-averaged and single-shot LIF OH images for the flat piston geometry (CAD given in frame title).

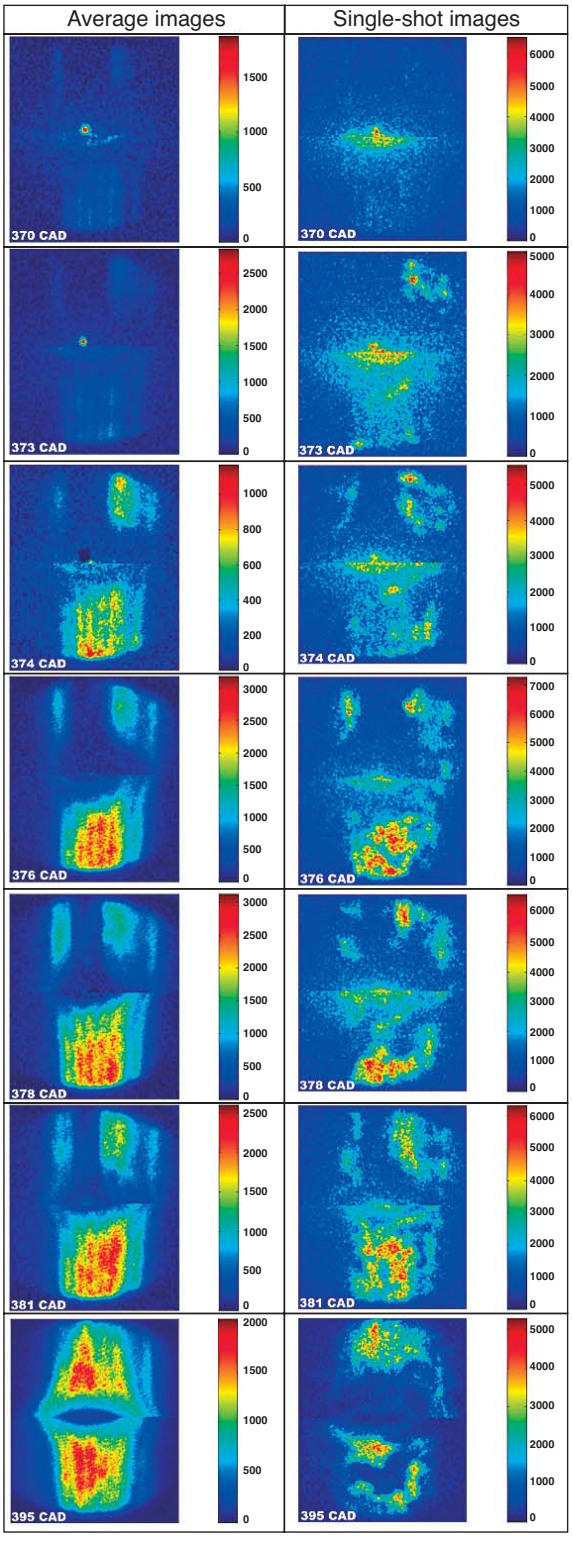

Figure 15

Ensemble-averaged and single-shot LIF OH images for the bowl-dome piston geometry (CAD given in frame title).

discussed earlier is believed to be due to PAH fluorescence. The lower graph in Figure 16 compares the temporal evolution of the LIF 355 signal relative to the OH fluorescence. One observes that the LIF OH signal has similar tendencies to the heat release rate. The LIF OH signal initially increases at the time when the LIF 355 signal (due to formaldehyde) starts to decrease. These results show that the two LIF techniques clearly identify the transition between the cool flame and the onset of main combustion during the two-stage HCCI combustion process.

Figure 17 presents the corresponding graphs of the mean LIF 355 and LIF OH signals for the bowl-dome geometry. Firstly, in considering the LIF 355 signal evolution in relation to the heat release rate, Figure 17 reveals, similarly to the results shown in Figure 16 that a peak LIF 355 signal is observed at about 370 CAD which shows excellent agreement with the small peak in the heat release. The origin of this signal, as described earlier is almost certainly due to the presence of reaction precursors such as formaldehyde which are intermediately formed by low temperature oxidation during the cool flame and subsequently consumed during the high temperature combustion stage. This is confirmed in Figure 17 which shows the signal decrease coinciding with the start of the main heat release from 372 CAD onwards and which is also similarly marked by the increase in the LIF OH signal. In comparing the LIF 355 signal to that of the flat piston geometry, the notable difference as discussed earlier is that later in the cycle there is no second peak associated to PAH fluorescence which is an indicator of the precursors of soot. These results again tend to indicate that the improved mixture homogeneity and in particular the absence of locally fuel-rich zones within the combustion chamber favourably improves the combustion process which is globally and locally more homogeneous

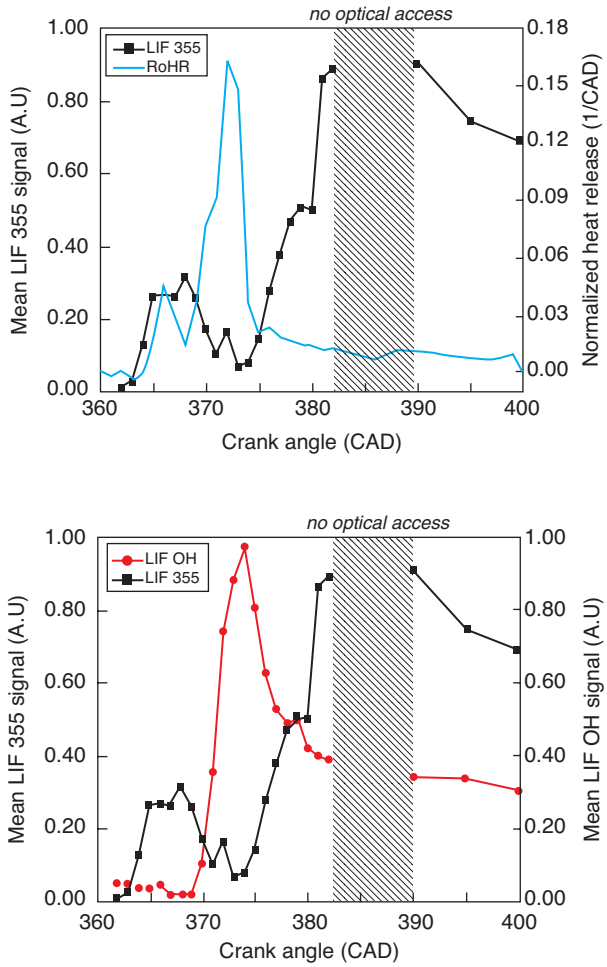

Figure 16

Comparison of the temporal evolution of the mean LIF 355 signal relative to the heat release rate (upper graph) and mean LIF OH signal (lower graph) for the flat piston geometry.

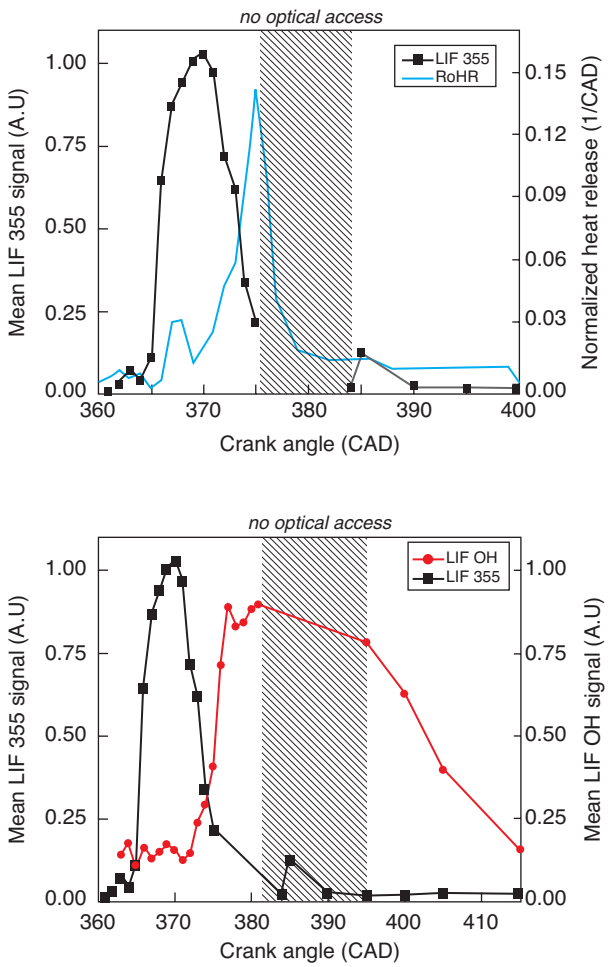

Figure 17

Comparison of the temporal evolution of the mean LIF 355 signal relative to the heat release rate (upper graph) and mean LIF OH signal (lower graph) for the bowl-dome piston geometry.

thereby limiting the peak combustion temperatures encountered which would explain the noticeable reductions in PAH and consequently engine-out soot emissions.

2.5 Spectrometry

In an attempt to identify the emitting species observed by direct chemiluminescence imaging, spectrometer measurements were performed. The results are presented for each piston geometry.

Figure 18 shows the evolution of the spectra obtained for the flat piston geometry during the early stages of combustion corresponding to the cool flame period between 365 and 372 CAD (upper graph) and later, during the hot flame at 380 and 385 CAD (lower graph). It is first of all clear from the spectra shown in Figure 18 that it was not possible to distinguish the presence and origin of radical species with precision due to the lack of resolution in the spectral bands and more importantly due to the low chemiluminescence signal-to-noise levels. However, the measured spectrum shown in Figure 18 clearly reveals a broad band peak centred around 430 nm at 372 CAD with several superimposed narrow, more closely spaced spectral bands. The emission spectra obtained during the cool flame are characteristic of the chemiluminescence emission of excited combustion radicals and in particular the emission of CH and CH_2O as reported elsewhere [6, 18, 21]. In contrast, later in the cycle, during the main combustion stage, the spectra obtained at 380 and 385 CAD are completely different and are more typical of the black body radiance emission resulting from sooting combustion which, in agreement with the images shown above corresponds to the very intense region observed in the centre of the piston and originates from the locally fuel-rich zone which was observed in the fuel vapour (LIEF) images discussed earlier in the paper.

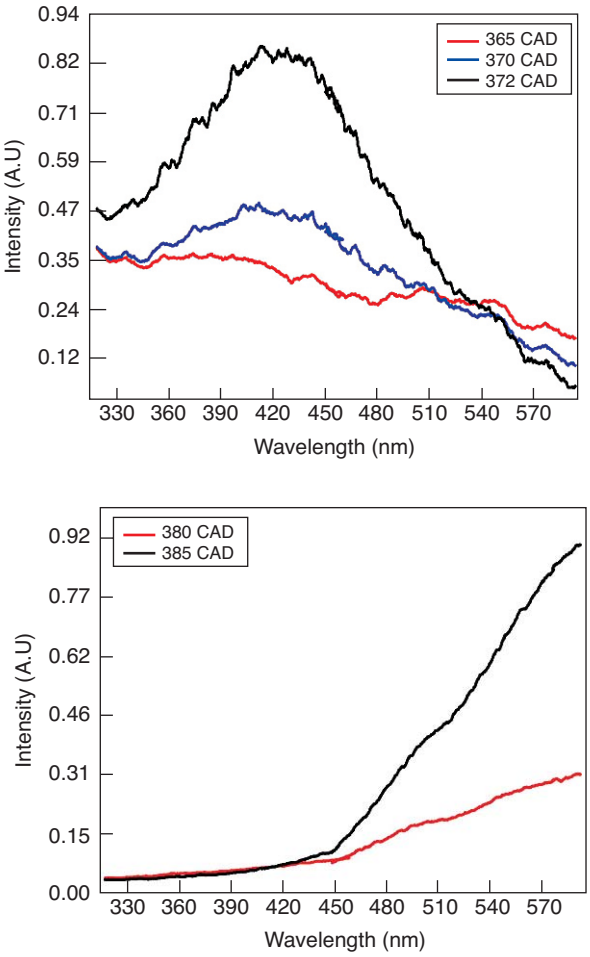

Figure 18

Chemiluminescence emission spectra measured during the cool flame (upper graph) & after the hot flame (lower graph) for the flat piston geometry.

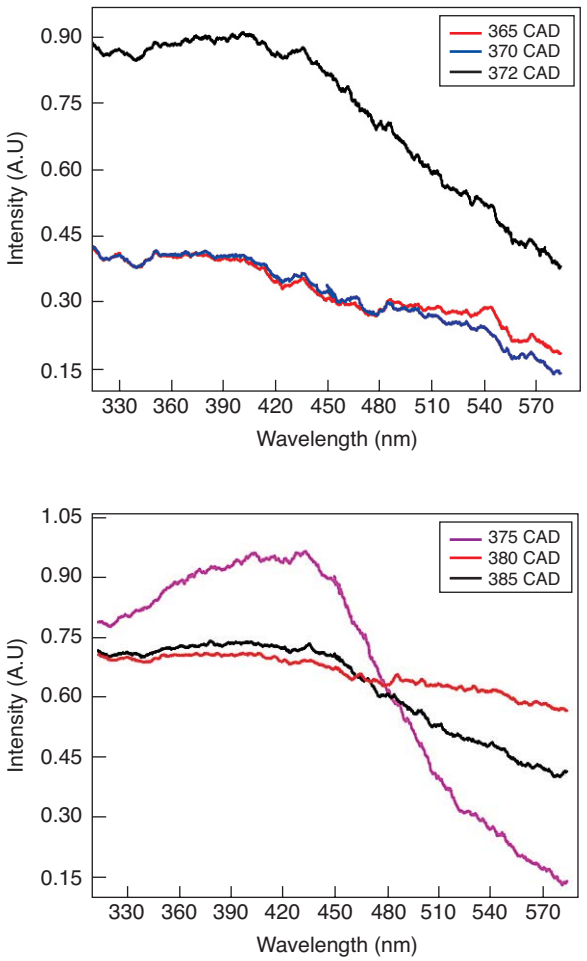

Figure 19

Chemiluminescence emission spectra measured during the cool flame (upper graph) & during/after the hot flame (lower graph) for the bowl-dome piston geometry.

Figure 19 shows the emission spectra obtained for the bowl-dome piston geometry which reveal significant differences in comparison to the flat piston. Firstly, the chemiluminescence spectra obtained during the cool flame between 365 and 372 CAD (upper graph) appear to be wide-band and continuous with no clearly defined peak at 430 nm although the smaller peaks superimposed on the wide-band spectrum indicate the likely presence of CH_2O. The differences in measured intensities observed could be an indicator of differences in equivalence ratio since it is reported [23] that the relative and absolute intensity of the various spectral band systems varies considerably with the mixture strength. The most notable difference is revealed later in the cycle, during the main combustion stage. The measured spectra between 375 and 385 CAD are still wide band and decrease progressively towards wavelengths of 570 nm. More importantly these spectra do not at all indicate the black body type radiance which is characteristic of sooting combustion as was observed in the case of the flat piston geometry. These results are in good agreement with the LIF 355 data obtained which, as shown earlier did not reveal PAH fluorescence which are the indicators of soot precursors late in the cycle.

SUMMARY AND CONCLUSIONS

The effect of piston geometry on the mixture preparation and combustion process has been studied in a direct injection HCCI Diesel engine. Laser induced exciplex fluorescence, chemiluminescence imaging and planar LIF of combustion radicals have been performed within a purpose-built, optically accessible piston bowl. The results presented indicate that piston geometry plays a significant role on the fuel mixture distribution within the piston bowl and on the subsequent combustion and emissions characteristics particularly for late injection HCCI strategies where liquid fuel impingement is unavoidable.

LIEF visualisations of the fuel distribution revealed that for the flat piston geometry, significant fuel impingement occurred which subsequently led to the formation of a locally fuel-rich region in the centre of the bowl. The resulting mixture stratification consequently had significant effects on the combustion process in terms of auto-ignition delay and the subsequent heat release rate. Planar LIF 355 images revealed the presence of the intermediate species formaldehyde just prior to auto-ignition and during the early cool flame stage between 361 and 372 CAD. Spectrometry measurements of the chemiluminescent light emission largely confirmed the fluorescing species to be that of formaldehyde. LIF 355 has also been shown to be a very useful diagnostic tool since it reveals the spatial location of auto-ignition precursors in advance of the initial weak chemiluminescence signal. Following the start of "hot" combustion after 373 CAD, a second, stronger signal was observed in the central region of the bowl in the case of the flat piston and was due to PAH fluorescence indicating the presence of soot precursors. Indeed, the combustion images obtained several crank angle degrees later confirmed the blackbody type radiance which is characteristic of sooting combustion whilst subsequent measurements by spectrometry also confirmed the significant presence of soot. Planar LIF imaging of the OH radical has also been applied as a means of identifying the spatial location and temporal evolution of the reaction and burned gas zones. The diminution of the LIF 355 signal and appearance of the initial LIF OH signal marked clearly the transition from the cool flame to the "hot" combustion phase whilst the LIF OH mean signal was found to follow closely the main heat release curve.

In contrast, the bowl-dome piston geometry was found to significantly improve mixture preparation as a result of convection of liquid fuel and vapour radially towards the bowl walls thereby enhancing fuel-air mixing and producing a globally more homogeneous mixture. This subsequently appeared to have a major influence on the combustion process. In particular, the bowl-dome combustion chamber geometry led to an increase in the auto-ignition delay which consequently reduced the pressure rise rate and peak in-cylinder pressure encountered. The improved mixture homogeneity attained is believed to be largely responsible for the significant reduction of soot during the latter stages of combustion in the case of the bowl-dome piston. This was later confirmed by spectrometry measurements. Single-shot and ensemble-averaged LIF 355 images revealed the presence of formaldehyde during the cool flame which was homogeneously distributed throughout the piston bowl. Later in the cycle, no PAH fluorescence was observed as was the case for the flat piston geometry which indicated the lower concentration of soot precursors. Planar LIF images of the OH radical obtained during the main combustion also indicated that combustion develops homogeneously throughout the chamber.

ACKNOWLEDGEMENTS

The authors would like to acknowledge Jean-François Papagni for maintaining the optical engine and Micheline Augé for assistance with the LIF OH experiments. This research was conducted within the framework of a research program funded by the Groupement Scientifique Moteurs *(IFP, PSA* and *Renault)*.

REFERENCES

1 Gray, A.W. and Ryan, T.W. (1997) Homogeneous Charge Compression Ignition (HCCI) of Diesel Fuel. SAE Paper 971676.

2 Stanglmaier, R.H. and Roberts, C.E. (1999) Homogeneous Charge Compression Ignition (HCCI): Benefits, Compromises and Future Engine Applications. SAE Paper 1999-01-3682.

3 Christensen, M., Johansson, B. and Einewall, P. (1997) Homogeneous Charge Compression Ignition (HCCI) using Isooctane, Ethanol and Natural Gas – A Comparison with Spark Ignition Operation. SAE Paper 972874.

4 Aceves, S.M., Flowers, D.L., Westbrook, CK., Pitz, W., Dibble, R., Christensen, M. and Johansson, B. (2000) A Multi-Zone Model for Prediction of HCCI Combustion and Emissions. SAE Paper 2000-01-0327.

5 Richter, M., Franke, A., Aldén, M., Hultqvist, A. and Johansson, B. (1999) Optical Diagnostics Applied to a Naturally Aspirated Homogeneous Charge Compression Ignition Engine. SAE Paper 1999-01-3649.

6 Dec, J.E. and Espey, C. (1995) Ignition and Early Soot Formation in a D.I. Diesel Engine Using Multiple 2-D Imaging Diagnostics. SAE Paper 950456.

7 Graf, N., Gronki, J., Schulz, C., Baritaud, T., Cherel, J., Duret, P. and Lavy, J. (2001) In-Cylinder Combustion Visualization in an Auto-Igniting Gasoline Engine Using Fuel-Tracer and Formaldehyde LIF Imaging. SAE Paper 2001-01-1924.

8 Thring, B. (1989) Homogeneous Charge Compression Ignition (HCCI) Engines. SAE Paper 892068.

9 Walter, B. and Gatellier, B. (2002) Development of the High Power NADI Concept Using Dual Mode Diesel Combustion to Achieve Zero NOx and Particulate Emissions. SAE Paper 2002-01-1744.

10 Melton, L.A. and Verdieck, J.F. (1985) Vapor/Liquid Visualization for Fuel Sprays. Comb. Sci. & Tech., 42, 217.

11 Melton, L.A. (1993) Exciplex-Based Vapor/Liquid Visualization Systems Appropriate for Automotive Gasolines, *Appl. Spectr.*, 47, 6.

12 Dec, J. and Coy, E.B. (1996) OH Radical Imaging in a DI Diesel Engine and the Structure of the Early Diffusion Flame. SAE Paper 960831.

13 Bockle, S., Kazenwadel, J., Kunzelmann, T., Shin, D.I., Schulz, C. and Wolfrum, J. (2000) Simultaneous Single-Shot Laser-Based Imaging of Formaldehyde, OH and Temperature in Turbulent Flames. *Proc. Comb. Inst.*, 28, pp. 279-286.

14 Bruneaux, G., Augé, M. and Lemenand, C. (2004) A Study of Combustion Structure in High-Pressure Single Hole Common Rail Direct Injection Using Laser Induced Fluorescence of Radicals. *Proc. COMODIA*, Yokohama, Japan, August.

15 Docquier, N. (2003) Influence of Fresh Charge Preparation and Composition on Auto-Ignition Delays and Combustion Development in an Optical HCCI Direct Injection Diesel Engine. SAE Paper 2003-01-3174.

16 Reveille, B., Miche, M., Jay, S. and Henriot, S. (2004) Contribution of 3D CFD Tools to the Development and Understanding of Diesel Engines: Improving Today's Engines and Designing Tomorrow's Power Units. Proc. SIA Int. congress, Lyon, France, May 12-14.

17 Heywood, J.B. (1988) *Internal Combustion Engine Fundamentals*. McGraw-Hill, New York.

18 Hultqvist, A., Christensen, M., Johansson, B., Franke, A., Richter, M. and Aldén, M. (1999) A Study of the Homogeneous Charge Compression Ignition Combustion Process by Chemiluminescence Imaging. SAE Paper 1999-01-3680.

19 Collin, R., Nygren, J., Richter, M., Aldén, M., Hildingsson, L. and Johansson, B. (2003) Simultaneous OH and Formaldehyde LIF Measurements in an HCCI Engine, SAE Paper 2003-01-3218.

20 Richter, M., Engstrom, J., Franke, A., Aldén, M., Hultqvist, A. and Johansson, B. (2000) The Influence of Charge Inhomogeneity on the HCCI Combustion Process. SAE Paper 2000-01-2868.

21 Kim, B., Kaneko, M., Ikeda, Y. and Nakajima, T. (2002) Detailed Spectral Analysis of the Process of HCCI Combustion. *Proc. Combust. Inst.*, 29, 671-677.

22 Puri, R., Santoro, R.J. and Smyth, K.C. (1994) The Oxidation of Soot and Carbon in Hydrocarbon Diffusion Flames. *Combustion and Flame*, **97**, 125-144.

23 Gaydon, A.G. (1974) *The Spectroscopy of Flames*, 2nd Ed., Chapman and Hall, London.

24 Tanaka, S., Ayala, F., Keck, J.C. and Heywood, J.B. (2003) Two-Stage Ignition in HCCI Combustion and HCCI Control by Fuels and Additives. *Combustion and Flame*, 132, pp. 219-239.

25 Dec, J.E. (2003) A Computational Study of the Effects of Low Fuel Loading and EGR on Heat Release Rates and Combustion Limits in HCCI Engines. SAE Paper 2002-01-1309.

26 Dec, J.E. and Sjöberg, M. (2004) Isolating the Effects of Fuel Chemistry on Combustion Phasing in an HCCI Engine and the Potential of Fuel Stratification for Ignition Control. SAE Paper 2004-01-0557.

Final manuscript received in November 2005